J. Phys.: Condens. Matter **22** (2010) 186002 (7pp) doi:10.1088/0953-8984/22/18/186002

Spin-wave dynamics of magnetic heterostructures: application to Dy/Y multilayers

J T Haraldsen and R S Fishman

Materials Science and Technology Division, Oak Ridge National Laboratory, Oak Ridge, TN 37831, USA

Received 13 January 2010, in final form 1 March 2010
Published 15 April 2010
Online at stacks.iop.org/JPhysCM/22/186002

Abstract

We examine the spin-wave (SW) dynamics of Dy/Y multilayers in order to separate the contribution of the Dy–Y interface from that of bulk Dy. The SW frequencies and intensities of bulk Dy are determined analytically. When the Dy layers in a multilayer geometry are decoupled, the SW dispersion relations are discontinuous with discrete excitations. With a Ruderman–Kittel–Kasuya–Yosida (RKKY) interaction coupling through the Y spacer, the discrete excitations become dispersive and the main SW branches split due to the multilayer geometry. Regardless of the strength of the intermediate RKKY interaction, the dispersion signature of the bulk remains.

(Some figures in this article are in colour only in the electronic version)

1. Introduction

Magnetic multilayers present unique opportunities for studying fundamental magnetic interactions [1–3]. Experimental developments in neutron scattering and epitaxial growth techniques have facilitated the production, control, and characterization of high-quality samples of multilayer heterostructures [4–7]. The availability of higher quality samples has accelerated theoretical and experimental work to clarify the intricate nature of these magnetic structures [6–12].

Interfaces between magnetic and non-magnetic layers exhibit a great variety of interesting magnetic behavior. Dzyaloshinskii–Moriya interactions induced by interfacial defects were recently studied to help explain the net chirality within multilayers observed using polarized neutron scattering [15, 16]. Other reports have shown that the Ruderman–Kittel–Kasuya–Yosida (RKKY) [12–14] interactions provide magnetic coherence through non-magnetic layers [10, 11]. A greater understanding of the magnetic properties and spin-wave (SW) dynamics of multilayer heterostructures can provide unique insight into the complex behavior of interfaces, supporting the advancement of magnetic based technologies and spintronics.

Due to their large local moments and complex magnetic ordering, rare-earth materials have been widely studied in both bulk and multilayer systems [2, 7]. These materials exhibit magnetic phenomena ranging from magnetostriction [17, 18] to multiple anisotropic properties [19] to spin chirality created by a Dzyaloshinskii–Moriya interaction [15]. The local moments in rare-earth materials typically form helical or conical magnetic structures [3]. These magnetic structures remain mostly intact in a multilayer system (shown in figure 1). Due to the large Dy moments and close lattice match between Dy and Y, bulk Dy and Dy/Y multilayers have attracted great interest [20–26, 35, 36].

Dy^{3+} has a magnetic moment of 10.6 μ_B with a $^6H_{15/2}$ ground state configuration [3]. The bulk crystal structure is known to form a hexagonal close packed (hcp) structure with lattice constants $a = 3.59$ Å and $c = 5.6$ Å, where $c/2$ is the spacing between Dy atomic layers. The magnetic structure undergoes two magnetic phase transitions at 140 K (paramagnetic to helical) and 87 K (helical to ferromagnetic) [22–24]. Within the helical phase, the local Dy moments form an in-plane helix with chirality parallel to the z-axis (shown in figure 1) and strong ferromagnetic interactions in-plane [3].

The helical structure of bulk Dy is produced by a competition between multiple antiferromagnetic and ferromagnetic super-exchange interactions [21]. As found by studying the SW dispersions, the exchange pathways extend through at least seven atomic Dy layers [21] (shown in figure 1). Observations of Dy/Ho multilayers have demonstrated that these interactions can propagate through magnetic Ho spacers [26]. Investigations of magnetic/non-magnetic Dy/Y multilayers revealed

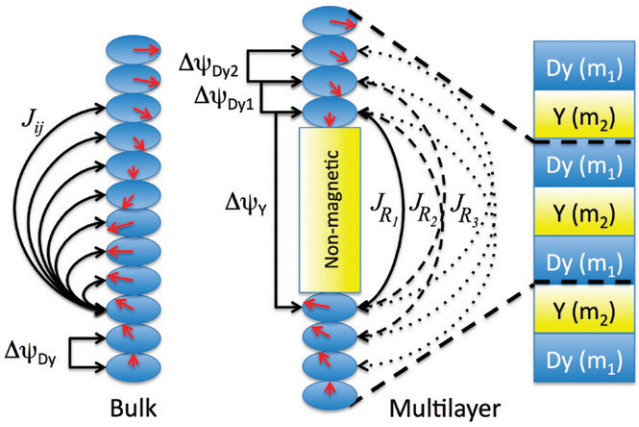

Figure 1. A pictorial representation of the in-plane helix in bulk Dy and the Dy/Y multilayer. J_{ij} describes the multiple Heisenberg interactions that are present in the Dy layer, while J_{R_1}, J_{R_2}, and J_{R_3} are the RKKY interactions through the Y spacer. $\Delta\psi$ denotes the different turn angles between magnetic sites.

that the helical nature of the Dy moments maintain coherence through the non-magnetic Y spacer [9].

In Dy/Y multilayers, the interaction between Dy atomic layers produces the same in-plane helicity as seen in the bulk. The suppression of the ferromagnetic phase allows the helical phase to remain stable to low temperatures. Rhyne *et al* [9] showed that the RKKY interactions mediated by the 4f electrons in the paramagnetic Y spacer create long-range helical coherence in the multilayer [10, 11]. While the strength of the RKKY coupling dramatically varies from antiferromagnetic to ferromagnetic due to the wavevector-dependent susceptibility, the RKKY interaction is modulated by a $1/R^3$ envelope [12]. This means that second- or third-order RKKY interactions may be larger than the first-order interaction, but that the interactions diminish quickly away from the interface.

Work on the SW dynamics of superlattices and multilayers has typically been restricted to investigations of the dispersion relations in specific multilayer structures with alternating ferromagnetic and antiferromagnetic layers [27–29]. Others have instituted long-wavelength approximations for periodic structures [30–34]. The goal of this paper is to gain a qualitative understanding of the effects of RKKY interactions in Dy/Y multilayers by calculating the SW frequencies and intensities through an exact diagonalization method, which is complicated by the incommensurate nature of the Dy local moments. This method allows us to simultaneously evaluate the SW frequencies and weights, thereby facilitating comparison with future measurements.

While the SW dynamics of the bulk rare-earth materials have been examined in great detail [3], detailed experimental and theoretical results on the SW dynamics of Dy/Y multilayers and other multilayers have not yet been published. Schreyer *et al* [35] presented data for the SW dispersions of Dy_{15}/Y_{10} multilayers. However, due to the weak inelastic signal, the data is limited to a small region of momentum and energy space.

In this paper, we examine the SW dynamics of Dy_{m_1}/Y_{m_2} multilayers, where m_1 and m_2 denote the number of Dy and Y atomic layers per bilayer, respectively as shown in figure 1. The SW frequencies and intensities for bulk Dy are presented in analytical form while the spin dynamics for the multilayer systems are solved numerically. As the systems transform from bulk to multilayer, the dispersion relations become discontinuous and discrete without a RKKY interaction. The RKKY interaction makes those individual excitations dispersive. A splitting of the SW branches is also caused by the bilayer thickness. Regardless of the strength of the intermediate RKKY interactions, the SW excitations follow the bulk dispersion. The RKKY interactions are examined in more depth in the appendix.

This paper is divided into five sections. Section 2 present the theoretical framework we use to evaluate the SW frequencies and intensities. In sections 3 and 4, the SW dynamics for bulk Dy and its multilayer counterpart are presented. Finally, the appendix details some of the calculations regarding the RKKY interactions.

2. Theory

Figure 1 illustrates the magnetic interactions in the bulk and multilayer systems. The bulk system is described by multiple competing Heisenberg interactions J_{ij} as well as an easy-plane anisotropy term D, which acts to keep the local moments in-plane. For a multilayer system, we also include the RKKY interactions J_{R_i} through the Y spacer. All of the interactions can be treated in a standard Heisenberg form.

Rare-earth systems are typically prone anisotropic magneto-elastic effects [18]. For Dy/Y multilayers the dominant crystal-field effects can be accounted for by the addition of an easy-plane anisotropy term D. Due to the incommensurate spin configuration in Dy, the spins do not lock with the hexagonal crystal field and the hexagonal magneto-elastic energy may by neglected [37]. This simplification allows us to focus on the main terms of the Hamiltonian while investigating the RKKY interactions.

Therefore, the Hamiltonian can be written as

$$H = -\tfrac{1}{2}\sum_{i\neq j} J_{ij}\mathbf{S}_i\cdot\mathbf{S}_j + D\sum_i \mathbf{S}_{iz}^2, \qquad (1)$$

where $\mathbf{S}_i$ is the local moment on site i and the exchange coupling J_{ij} between sites i and j is antiferromagnetic when $J_{ij} < 0$. We are primary interested in the SW dynamics along the z-axis, which allows spins in each layer to be treated rigidly. While hexagonal anisotropy, magneto-elastic, and Dzyaloshinskii–Moriya interactions may be present, these terms are often small and can be ignored for an incommensurate helical spin state if the interfaces are perfect [15, 16, 22, 24].

Using a Holstein–Primakoff (HP) transformation, the spin operators are given by $S_{iz} = S - a_i^\dagger a_i$, $S_{i+} = \sqrt{2S}a_i$, and $S_{i-} = \sqrt{2S}a_i^\dagger$. A rotation of the operators adjusts for the in-plane local moments [38]. Expanding about the classical limit in powers of $1/\sqrt{S}$, the Hamiltonian can be written as $H = E + H_1 + H_2 + \cdots$. Since the first-order term H_1 vanishes

with a minimization of the energy E, the second-order term H_2 provides the dynamics of non-interacting SWs. Higher-order terms $H_{n>2}$ reflect the interactions between SWs, which are unimportant at low temperature and for small $1/S$. Due to the large Dy spin, we expect the HP transformation to be quite accurate.

To determine the SW frequencies $\omega_{\mathbf{q}}$, we solve the equation-of-motion for the vectors $\mathbf{v_q} = [a_{\mathbf{q}}^{(1)}, a_{\mathbf{q}}^{(1)\dagger}, a_{\mathbf{q}}^{(2)}, a_{\mathbf{q}}^{(2)\dagger}, \ldots]$, which may be written in terms of the $2N \times 2N$ matrix $\underline{M}(\mathbf{q})$ as $\mathrm{id}\mathbf{v_q}/\mathrm{d}t = -[\underline{H}_2, \mathbf{v_q}] = \underline{M}(\mathbf{q})\mathbf{v_q}$, where N is the number of spin sites in the unit cell [38]. The SW frequencies are then determined from the condition $\mathrm{Det}[\underline{M}(\mathbf{q}) - \omega_{\mathbf{q}}\underline{I}] = 0$. Two conditions are required for the local stability of any magnetic phase: all SW frequencies must be real and positive and all SW weights must be positive.

The SW intensities or weights are coefficients of the spin–spin correlation function:

$$S(\mathbf{q}, \omega) = \sum_{\alpha\beta}(\delta_{\alpha\beta} - \mathbf{q}_\alpha \mathbf{q}_\beta) S^{\alpha\beta}(\mathbf{q}, \omega), \tag{2}$$

where α and β can be $+$, $-$, or z. Here, $S^{+-}(\mathbf{q}, \omega)$ and $S^{-+}(\mathbf{q}, \omega)$ are the transverse terms reflecting fluctuations in the xy-plane. The longitudinal term $S^{zz}(\mathbf{q}, \omega)$ creates fluctuations along the z-axis, which are produced by the in-plane structure of the local moments [39]. A more detailed discussion of the longitudinal and transverse modes can be found in [38, 39]. It should be noted that inelastic neutron scattering measurements will only observe the components of the weight that are perpendicular to the $\mathbf{q}$ vector [41]. Because the helix lies in the xy-plane, most measurements of rare-earth multilayers have been performed along the q_z direction. Therefore, the longitudinal $S^{zz}(\mathbf{q}, \omega)$ component will not be observed.

The total intensity $I(\mathbf{q}, \omega)$ for inelastic neutron scattering scans at constant $\mathbf{q}$ is given by

$$I(\mathbf{q}, \omega) = S(\mathbf{q}, \omega) F_{\mathbf{q}}^2 \mathrm{e}^{\frac{-(\omega-\omega_{\mathbf{q}})^2}{2\delta^2}}, \tag{3}$$

where δ is the energy resolution and $F_{\mathbf{q}}$ is the Dy^{3+} ionic form factor [40][1]. Here, the simulated energy resolution is based on a Gaussian distribution, which is standard for constant $\mathbf{q}$ scans on a triple-axis spectrometer [41, 42]. Other configurations may need more complex resolution functions.

Hence, we also focus on the case of $\mathbf{q}$ along the z-axis with $q_x = q_y = 0$. Since only the exchange interactions J_{ij} coupling the neighboring layers will contribute to the excitations, numerical solutions of the frequencies and intensities are determined by diagonalizing a $2m_1 \times 2m_1$ matrix.

3. Bulk dysprosium

While bulk materials have been examined in great detail [3, 20, 21], an expression for the SW intensities of bulk Dy has not been presented. Previous literature has only reported the lower transverse branch of bulk Dy [20] and not the middle longitudinal branch in figure 2.

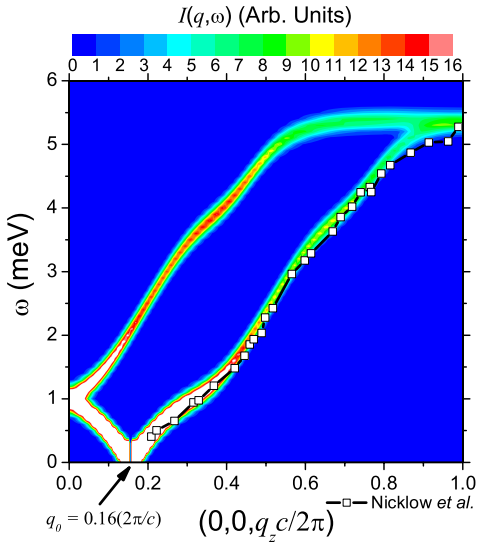

Figure 2. Calculated contour plot of $I(\mathbf{q}, \omega)$ for bulk Dy using the parameters determined by [21]. The white contours are regions of high intensity (>16) and q_0 denotes the helical wavevector of $0.16(2\pi/c)$. An energy resolution of 0.1 meV was simulated using a standard Gaussian function. The open black squares show the experimental dispersion data points observed by Nicklow *et al* [21][2] .

Because the local moments of bulk Dy are in the xy plane, the SW frequencies are given by

$$\omega_{\mathbf{q}} = S\sqrt{A_1^2 - A_2^2}, \tag{4}$$

where

$$A_1 = \sum_n J_n[2\cos(n\Delta\psi_n) - \cos(\tau \cdot d_n)(1 + \cos(n\Delta\psi_n))], \tag{5}$$

$$A_2 = \sum_n J_n[\cos(\tau \cdot d_n)(1 - \cos(n\Delta\psi_n)) + D_n], \tag{6}$$

where $\Delta\psi_n$ is the turn angle or change in azimuthal angle for interaction n between sites i and j, d_n is the interaction distance, and τ is the momentum transfer. The functional form for all branches are equivalent with only a shift in the momentum transfer relating to the helical wavevector. This is consistent with expressions determined by Nicklow *et al* [21] (see footnote 2) for the transverse branches. The longitudinal branch corresponds to $\tau = q$ and the transverse branches are $\tau = q \pm q_0$.

The helical wavevector q_0 can be determined from the general relationship

$$\sum_n n J_n \sin\left(\frac{n q_0 c}{2}\right) = 0. \tag{7}$$

[1] The Dy^{3+} magnetic form factor is given as $F_{\mathbf{q}} = j_0(\mathbf{q}) + (1 - 2/g_{\mathrm{Dy}})j_2(\mathbf{q})$, where $g_{\mathrm{Dy}} = 4/3$, $j_0(\mathbf{q}) = A_0\mathrm{e}^{a_0 s^2} + B_0\mathrm{e}^{b_0 s^2} + C_0\mathrm{e}^{c_0 s^2} + D_0$, $j_2(\mathbf{q}) = s^2(A_2\mathrm{e}^{a_2 s^2} + B_2\mathrm{e}^{b_2 s^2} + C_2\mathrm{e}^{c_2 s^2} + D_2)$ and $s = \sin\theta/\lambda = \mathbf{q}/4\pi$. The coefficients are given as $A_0 = 0.1157$ ($a_0 = 15.0732$), $B_0 = 0.3270$ ($b_0 = 6.7991$), $C_0 = 0.5821$ ($c_0 = 3.0202$), $D_0 = -0.0249$, $A_2 = 0.2523$ ($a_2 = 18.5172$), $B_2 = 1.0914$ ($b_2 = 6.7362$), $C_2 = 0.9345$ ($c_2 = 2.2082$) and $D_2 = 0.0250$ from [40].

[2] Data presented by Nicklow *et al* [20, 21] is shifted by q_0 due to the reduced wavevector notation used in those papers.

If $n = 2$ (the minimum number of interactions required), then the helical wavevector is [2]

$$\cos\left(\frac{q_0 c}{2}\right) = \frac{-J_1}{4J_2}, \tag{8}$$

in which case the interactions must be of opposite sign and the helix is only stable when $|J_1| \geqslant 4|J_2|$. With bulk Dy described by seven interactions [21], the helical wavevector is about 0.16 $(2\pi/c)$.

The SW intensities (weights) are determined from the SW frequencies for the transverse and longitudinal branches can be written as

$$I(\mathbf{q}, \omega)^{\pm} = F_{\mathbf{q}}^2 \frac{S(A_1 \pm A_2)}{\omega_{\mathbf{q}}} e^{\frac{-(\omega-\omega_{\mathbf{q}})^2}{2\delta^2}}, \tag{9}$$

where $\pm$ denotes the transverse $(+)$ and longitudinal $(-)$ branches, respectively. In the limit of $\tau \to 0$, the longitudinal intensity approaches zero, while the transverse branches diverge.

Figure 2 shows the calculated SW dispersion for bulk Dy as an intensity contour as a function of energy and momentum transfer. The exchange interactions are those given in table I of [21]. An energy resolution $\delta = 0.1$ meV is used to simulate experimental resolution. The black boxes show the comparison to the data provided by Nicklow *et al* [21]. These branches are produced by the transverse components of the intensity. As explained above, the longitudinal component would not be observed with **q** along the z-axis.

4. Dy/Y multilayers

In bulk Dy, the turn angle between neighboring Dy sites is essentially constant and experimentally found to be about $\sim 28°$. In Dy_{m_1}/Y_{m_2} multilayers, m_1 Dy atomic layers are separated by a spacer of m_2 Y atomic layers (shown in figure 1). The Dy sites near the non-magnetic spacer are influenced by different interactions than the sites in the middle of the Dy layer. Our calculations find that the turn angles between Dy atomic layers $\Delta\psi_{\mathrm{Dy}}$ are smaller near the Y spacer interface and then widen to give an average turn angle of $\sim 30°$. Due to the presence of a RKKY interaction, the induced helical coherence is modeled by an overall turn angle through the Y spacer $\Delta\psi_{\mathrm{Y}}$ as shown in figure 1. Experimentally [9], this turn angle is about $m_2 \cdot 51°$. Minimizing the classical energy (detailed in appendix), the Y turn angle can be determined in terms of the RKKY interactions.

Figure 3 shows J_{R_2} as a function of J_{R_1} needed to obtain a $m_2 \cdot 51°$ turn angle through the Y spacer for various J_{R_3} interactions. The RKKY interactions describe the interlayer coupling as illustrated in figure 1. The nonlinear relationship between J_{R_2} and J_{R_1} implies that the turn angle is not a simple function of the ratio J_{R_2}/J_{R_1}. The inset to figure 3 demonstrates how $\Delta\psi_{\mathrm{Y}}$ depends on J_{R_2} for various values of J_{R_1}. Figure 3 demonstrates that many combinations of RKKY interactions can produce the same turn angle $\Delta\psi_{\mathrm{Y}}$. It is not surprising that J_{R_2} is comparable J_{R_1} since they both involve RKKY interactions passing through the same Y spacer.

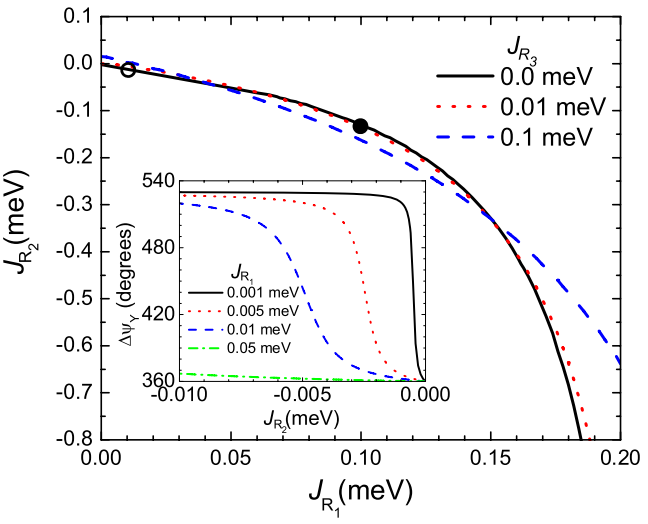

Figure 3. J_{R_2} as a function of J_{R_1} needed to obtain a $m_2 \cdot 51°$ turn angle through the Y spacer for various values of J_{R_3}. The inset shows the Y space turn angle as a function of J_{R_2} for different values of J_{R_1} with $m_2 = 10$. The circles denote the values of J_{R_1} and J_{R_2} used for the middle (open circle) and right (solid circle) panels in figure 4. All RKKY interactions are illustrated in figure 1.

Comparison with experimental results for the SW dynamics is required to determine the precise RKKY interactions involved within these multilayers.

As m_2/m_1 increases, it is expected that the SW dynamics will deviate from the bulk limit. Figures 4(a)–(c) shows the calculated SW dispersion contours for Dy_{m_1}/Y_{10} multilayers with $m_1 = 40$ (a), 30 (b), and 15 (c) for various RKKY interactions. The left panels contain no RKKY interaction, while the middle and right panels have $J_{R_1} = 0.010$ meV ($J_{R_2} = -0.0076$ meV) and $J_{R_1} = 0.10$ meV ($J_{R_2} = -0.13$ meV), respectively. These calculations were performed with $J_{R_3} = 0$. Using figure 3, J_{R_1} and J_{R_2} were constrained to produce the appropriate turn angle through the Y spacer, which is denoted by an open (middle panels) or a solid (right panels) circle. Intralayer interactions are given by those found in [21]. An energy resolution $\delta = 0.1$ meV is used to simulate experimental resolution.

Since the overall magnitude of the RKKY interactions decreases as the number of non-magnetic sites increases [10, 11], the Y spacer thickness alters the RKKY interaction. When $m_2 \gg m_1$, the RKKY interaction would vanish, creating the same discrete excitations seen in left panels of figure 4. In contrast, as m_2 is reduced, the dispersion become more bulk-like. While the strength of the RKKY interactions vary from antiferromagnetic to ferromagnetic [10, 11], it is important to consider a constant Y spacer thickness to understand the effects of the RKKY interactions on the system.

Without a RKKY interaction, the multilayer spectra still resembles the bulk dispersion in q space. With $m_1 = 4m_2$ (figure 4(a)), the dispersion shows the presence of small steps of discrete excitations. As m_1 is decreased and approaches m_2, the discrete excitations become more evident. This is expected, since a system with no RKKY interaction would essential be a cluster chain in the z-direction. The mimicking

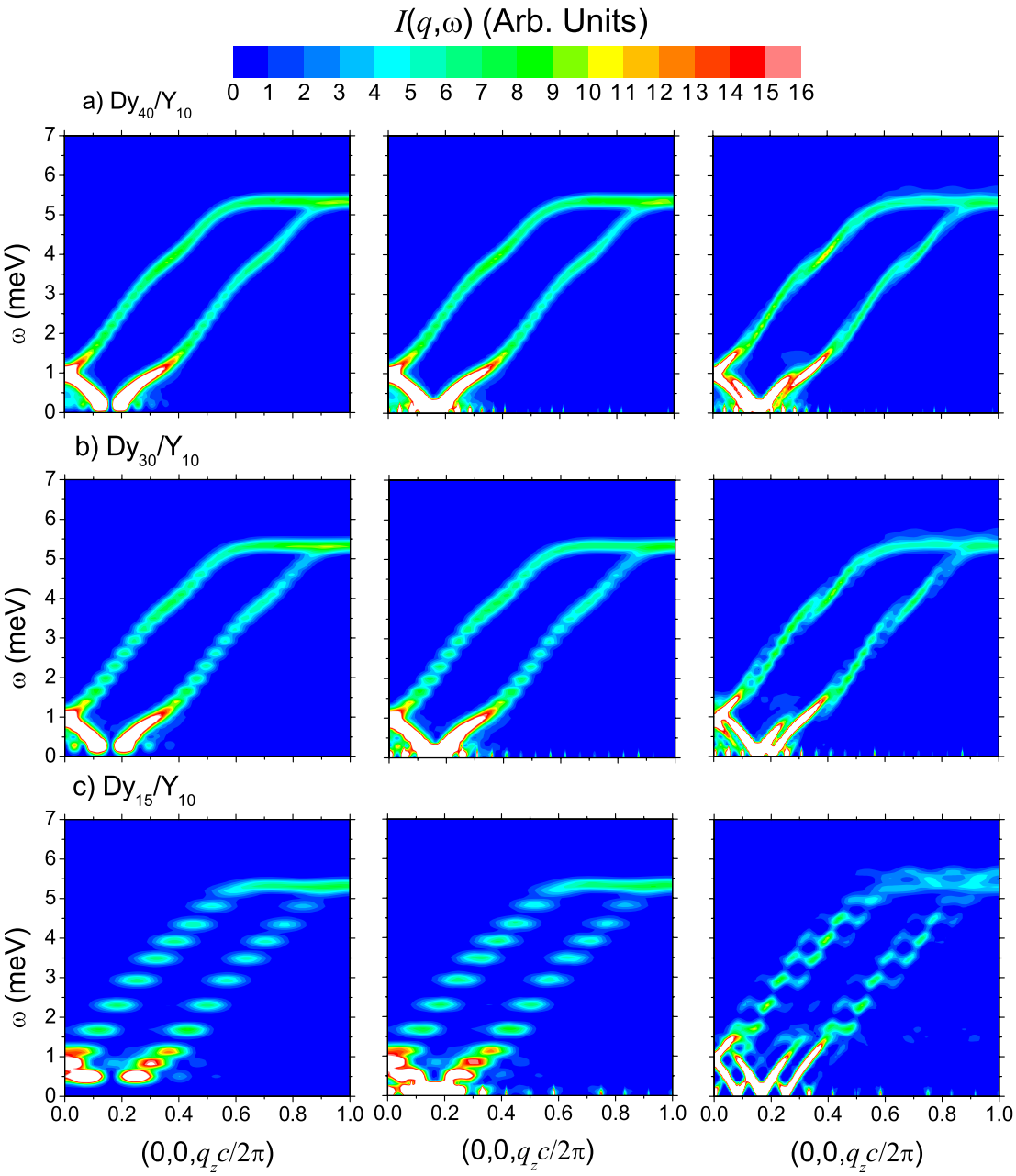

Figure 4. Calculated contour plots of $I(\mathbf{q}, \omega)$ for multilayers of Dy_{40}/Y_{10} (a), Dy_{30}/Y_{10} (b), Dy_{15}/Y_{10} (c) with no RKKY (left panels), $J_{R_1} = 0.010$ and $J_{R_2} = -0.0076$ meV (middle panels), and $J_{R_1} = 0.10$ and $J_{R_2} = -0.13$ meV (right panels). The energy of each system has been minimized to produce $\Delta\psi_Y = m_2 \cdot 51°$. Using $J_{R_3} = 0.0$, J_{R_2} is determined from open (middle panels) and solid (right panels) circles in figure 3. The white contours are regions of high intensity (>16). These simulations use $\delta = 0.1$ meV.

of the bulk dispersion is due to the helical dependence on the interactions. As m_1 decreases, the discrete excitations become more prominent and the system begins to lose the bulk signature.

In the left panels of figure 4, m_1 discrete energy levels have an average spacing of $\Delta\omega \sim 5\omega_{max}/4m_1$ with the top $m_1/5$ levels being semi-degenerate[3]. As $m_1 \to \infty$, the discrete levels become a continuum of excitations describing the behavior of the bulk system. This bulk-like dispersion can also be retrieved by activating a RKKY interaction through the non-magnetic spacer.

As shown in right panels of figure 4, the presence of a RKKY interaction creates dispersion of the discrete excitations. This effect is more prominent as the interactions gain strength and coherence through the non-magnetic Y spacer (middle to right panels). However, the dispersion lines shift from the bulk signature and produce breaks in the spectrum as the RKKY interaction is increased in strength comparable to the intralayer interactions. These breaks are to be caused by the bilayer periodicity of the multilayer. As m_1 becomes smaller, the branches move further apart and become

[3] $\Delta\omega \sim 5\omega_{max}/4m_1$ is only an average spacing for the excitations. The low energy excitations tend to group closer as does the higher energy levels, while the middle range excitations tend to spread out in energy space.

less bulk-like due to decreasing bilayer size. This reveals the importance of examining the spin dynamics to assess the strength of relevant RKKY interactions.

Notice the excitations at ∼5.5 meV in the lower-right panel of figure 4. These features seem to arise from excitations through the non-magnetic Y spacers when the RKKY interaction is large. By changing the ratio between the interactions or through the addition of extra RKKY interactions, these excitations shift in energy and momentum space. While these are qualitative results, this indicates that it may be possible to directly probe the RKKY interactions through the Y spacer. Future work is intended to investigate these excitation and gain a quantitative understanding them as well as compare to experimental data on these multilayers.

While some work has been performed on Dy_{15}/Y_{10} multilayers [35], more detailed experiments on a wider range of multilayers is need. Current inelastic neutron scattering measurements are underway at Oak Ridge National Laboratory on D_{40}/Y_{10} multilayers.

5. Conclusions

To help understand the behavior of magnetic multilayers, we follow the evolution of the SW dispersions as bulk Dy progresses to a multilayer. As the system moves away from the bulk system, discrete excitations begin to form, but the overall bulk signature is still present. A RKKY interaction through the Y spacer enables coherence of the helical spin state throughout the multilayer. This produces dispersion in the discrete excitations, while larger RKKY interactions start to break the dispersions into multiple SW branches. The spacing of the branches is related to the bilayer spacing, where the RKKY interactions also produce well-defined structures in the SW dynamics, which makes it possible to experimentally determine the RKKY interactions from inelastic neutron scattering measurements. Future inelastic measurements on Dy/Y multilayers will help clarify the complex interactions at the interface between magnetic and non-magnetic materials.

Acknowledgments

Special thanks to S Okamoto and A Schreyer for insightful discussions. This research was sponsored by the Laboratory Directed Research and Development Program of Oak Ridge National Laboratory, managed by UT-Battelle, LLC for the US Department of Energy under Contract No. DE-AC05-00OR22725 and by the Division of Materials Science and Engineering and the Division of Scientific User Facilities of the US DOE.

Appendix. RKKY interactions

The classical energy for a Dy/Y multilayer with m_1 Dy atomic layers can be separated into Heisenberg interactions (intralayer interactions) and RKKY interactions (interlayer interactions) written as

$$E_0 = \sum_{ij} J_{ij}\cos(\Delta\psi_{ij}) + \sum_{ij} J_{R_{ij}}\cos(\Delta\psi_{ij}), \qquad (A.1)$$

where $\Delta\psi_{ij}$ is the change in azimuthal angle for interaction J_{ij} or $J_{R_{ij}}$. Due to the presence of an RKKY interaction through the non-magnetic spacer, a subsequent turn angle $\Delta\psi_Y$ is introduced to account for the effective twist of the helix within the Y spacer. Since only the interlayer interactions involve $\Delta\psi_Y$, the classical energy can be written as

$$\begin{aligned} E_0 = {} & J_{R_1}\cos(\Delta\psi_Y) + 2J_{R_2}\cos(\Delta\psi_Y + \Delta\psi_{Dy_1}) \\ & + J_{R_3}[2\cos(\Delta\psi_Y + \Delta\psi_{Dy_1} + \Delta\psi_{Dy_2}) \\ & + \cos(\Delta\psi_Y + 2\Delta\psi_{Dy_1})] + \cdots, \end{aligned} \qquad (A.2)$$

where $\Delta\psi_{Dy_1}$ and $\Delta\psi_{Dy_2}$ are the turn angles for the nearest and next nearest Dy–Dy interaction and J_{R_i} are the RKKY interactions described in figure 1. The RKKY coupling are defined in figure 1 as the interlayer nearest neighbor interactions.

By minimizing the classical energy with respect to $\Delta\psi_Y$ angle, we obtain

$$\frac{\sin(\Delta\psi_Y)}{\sin(\Delta\psi_Y + \Delta\psi_{Dy_1})} = \frac{-2J_{R_2}}{J_{R_1}}. \qquad (A.3)$$

Therefore, the interaction ratio depends on the Y turn angle and the first Dy turn angle. As more RKKY interactions are introduced into the Hamiltonian, the relationship becomes more complex. For three RKKY interactions, the relationship is

$$\begin{aligned} & \tan(\Delta\psi_Y + \Delta\psi_{Dy_1}) \\ & = \frac{\sin(\Delta\psi_{Dy_1})(J_{R_1} - J_{R_3}) - 2J_{R_3}\sin(\Delta\psi_{Dy_2})}{2J_{R_2} + \cos(\Delta\psi_{Dy_1})(J_{R_1} + J_{R_3}) + 2J_{R_3}\cos(\Delta\psi_{Dy_2})}. \end{aligned} \qquad (A.4)$$

For the simulations shown in figure 4, only two RKKY interactions were considered since that is the minimal number needed to create a turn angle through the Y spacer.

References

[1] Bennett L H and Watson R E 1994 *Magnetic Multilayers* (New Jersey: World Scientific)
[2] Elliott R J 1961 *Phys. Rev.* **124** 346
[3] Elliot R J 1972 *Magnetic Properties of Rare Earth Metals* (New York: Plenum)
[4] Gibson J H and Dawson L R 1965 *Layered Structures, Epitaxy and Interfaces* (Pittsburgh, PA: Mater. Res. Soc.)
[5] Hong M, Wolf S and Gubser D 1988 *Metallic Multilayers and Epitaxy* (Warrendale, PA: The Metallurgical Society)
[6] Mangin Ph, Dufour C and Rodmacq B 1993 *Physica* B **192** 122
[7] Majkrzak C F 1996 *Physica* B **221** 342
[8] Albuquerque E L, Fulco P, Sarmento E F and Tilley D R 1986 *Solid State Commun.* **58** 41
[9] Rhyne J J, Erwin R W, Borchers J, Shinha S, Salamon M B, Du R and Flynn C P 1987 *J. Appl. Phys.* **61** 4043
[10] Yafet Y 1987 *J. Appl. Phys.* **61** 4058
[11] Yafet Y, Kwo J, Hong M, Majkrzak C F and O'Brien T 1988 *J. Appl. Phys.* **63** 3453
[12] Ruderman M A and Kittel C 1954 *Phys. Rev.* **96** 99
[13] Kasuya T 1956 *Prog. Theor. Phys.* **16** 45
[14] Yosida K 1957 *Phys. Rev.* **106** 893
[15] Grigoriev S V, Chetverikov Yu O, Lott D and Schreyer A 2008 *Phys. Rev. Lett.* **100** 197203

[16] Haraldsen J T and Fishman R S 2010 *Phys. Rev.* B **81** 020404(R)
[17] Clark A E, DeSavage B F and Bozorth R 1965 *Phys. Rev.* **138** A216
[18] Rosen M and Klimker H 1970 *Phys. Rev.* B **1** 3748
[19] Rhyne J J and Clark A E 1967 *J. Appl. Phys.* **38** 1379
[20] Nicklow R M 1971 *J. Appl. Phys.* **42** 1672
[21] Nicklow R M, Wakabayashi N, Wilkinson M K and Reed R E 1971 *Phys. Rev. Lett.* **26** 140
[22] Liu S H, Behrendt D R, Legvold S and Good R H Jr 1959 *Phys. Rev.* **116** 1464
[23] Wilkinson M K, Koehler W C, Wollan E O and Cable J W 1961 *J. Appl. Phys.* **32** 48S
[24] Cooper B R 1962 *Proc. Phys. Soc.* **80** 1225
[25] Simpson J A, Cowley R A, McMorrow D F, Ward R C C, Wells M R, Carlile C J and Adams M A 1996 *J. Phys.: Condens. Matter* **8** L187
[26] del Moral A, da la Fuente C, Arnaudas J I, Ciria M, Benito L, Wells M R and Ward R C C 2001 *J. Magn. Magn. Mater.* **226** 1700
[27] Stamps R L and Camley R E 1996 *Phys. Rev.* B **54** 15200
[28] Oliveros M C, Almeida N S, Tilley D R, Thomas J and Camley R E 1992 *J. Phys.: Condens. Matter* **4** 8497
[29] Qiu R, Song P and Zhang Z 2009 *J. Magn. Magn. Mater.* **321** 3031
[30] Hinchey L L and Mills D L 1986 *Phys. Rev.* B **33** 3329
[31] Wang X-Z and Tilley D R 1995 *Phys. Rev.* B **52** 13353
[32] Wang R W and Mills D L 1994 *Phys. Rev.* B **50** 3931
[33] Wang R W and Mills D L 1996 *Phys. Rev.* B **53** 2627
[34] Trallori L, Politi P, Rettori A and Pini M G 1995 *J. Phys.: Condens. Matter* **7** 7561
[35] Schreyer A, Schmitte T, Siebrecht R, Bodeker P, Zabel H, Lee S H, Erwin R W, Majkrzak C F, Kwo J and Hong M 2000 *J. Appl. Phys.* **87** 5443
[36] Majkrzak C F, Kwo J, Hong M, Yafet Y, Gibbs D, Chien C L and Bohr J 1991 *Adv. Phys.* **40** 99
[37] Evenson W E and Liu S H 1969 *Phys. Rev.* B **178** 783
[38] Haraldsen J T and Fishman R S 2009 *J. Phys.: Condens. Matter* **21** 216001
[39] Squires G L 1978 *Introduction to the Theory of Thermal Neutron Scattering* (New York: Dover)
[40] Dianoux A J and Lander G 2003 *Neutron Data Booklet* (Philadelphia, PA: OCP Science)
[41] Shirane G, Shapiro S M and Tranquada J M 2002 *Neutron Scattering with a Triple-Axis Spectrometer* (Cambridge: Cambridge University Press)
[42] Chesser N J and Axe J D 1973 *Acta Crystallogr.* A **29** 160